

The major facilitator superfamily member Slc37a2 is a novel macrophage-specific gene selectively expressed in obese white adipose tissue

Ji Young Kim, Kristin Tillison, Shengli Zhou, Yu Wu and Cynthia M. Smas

Am J Physiol Endocrinol Metab 293:E110-E120, 2007. First published 13 March 2007;

doi:10.1152/ajpendo.00404.2006

You might find this additional info useful...

This article cites 58 articles, 20 of which can be accessed free at:

<http://ajpendo.physiology.org/content/293/1/E110.full.html#ref-list-1>

Updated information and services including high resolution figures, can be found at:

<http://ajpendo.physiology.org/content/293/1/E110.full.html>

Additional material and information about *AJP - Endocrinology and Metabolism* can be found at:

<http://www.the-aps.org/publications/ajpendo>

This information is current as of October 21, 2011.

The major facilitator superfamily member Slc37a2 is a novel macrophage-specific gene selectively expressed in obese white adipose tissue

Ji Young Kim, Kristin Tillison, Shengli Zhou, Yu Wu, and Cynthia M. Smas

Department of Biochemistry and Cancer Biology, Medical University of Ohio, Toledo, Ohio

Submitted 8 August 2006; accepted in final form 12 March 2007

Kim JY, Tillison K, Zhou S, Wu Y, Smas CM. The major facilitator superfamily member Slc37a2 is a novel macrophage-specific gene selectively expressed in obese white adipose tissue. *Am J Physiol Endocrinol Metab* 293: E110–E120, 2007. First published March 13, 2007; doi:10.1152/ajpendo.00404.2006.—A marked degree of macrophage infiltration of white adipose tissue (WAT) occurs in obesity and may link excess adiposity with the chronic inflammatory state underlying metabolic syndrome and other comorbidities of obesity. Excess deposition of fat in the intra-abdominal vs. subcutaneous WAT depots is a key component of metabolic syndrome. Through construction and differential screening of a murine *ob/ob* WAT cDNA library, we identified Slc37a2, a novel sugar transporter of the major facilitator superfamily, to be twofold enriched in intra-abdominal vs. subcutaneous fat. We find Slc37a2 is a macrophage-enriched transcript. In murine tissues, Slc37a2 transcript is restricted to spleen, thymus, and obese WAT. It is also readily detected in the RAW264.7 macrophage cell line and increases 46-fold during macrophage differentiation of THP-1 human monocytes. Compared with wild-type mice, Slc37a2 transcript is increased epididymal ninefold in *ob/ob* WAT and assessment of expression of the macrophage marker *emr1* indicated upregulation of Slc37a2 transcript in macrophages populating *ob/ob* WAT. Studies with PNGase F and tunicamycin reveal the Slc37a2 protein is posttranslationally modified by addition of N-linked glycans. Slc37a2 protein migrates as heterogeneous species of ~50–75 kDa and its ectopic expression in mammalian cells results in the appearance of large intracellular vacuoles. We postulate that the function of this macrophage-specific putative sugar transporter is central to the metabolism of the macrophage population specifically present in obese WAT.

obesity; sugar transporter

WHITE ADIPOSE TISSUE (WAT) is recognized to have multiple functions that are not only related to the storage of excess energy intake and its mobilization but also the secretion of hormones and adipokines (2, 13, 21, 29). Obesity is related to a number of health risks including insulin resistance, type 2 diabetes, cardiovascular disease, and some types of cancers (1, 12, 57). Studies to date indicate that different WAT depots evidence distinctions in, for example, gene expression and lipolytic response, among others (16, 27, 34, 35, 42, 50, 52–55). A relationship between the regional distribution of body fat and the comorbidities of obesity has recently been recognized. Intra-abdominal adiposity correlates with obesity-associated disorders, for example the metabolic syndrome, to a higher degree than the accumulation of fat in the subcutaneous WAT depots (7, 27). Interventions that target reduction of intra-abdominal fat mass effectively combat obesity-related diseases (24).

WAT is a heterogeneous organ with adipocytes estimated to comprise two-thirds of the WAT cell population; the remaining cell types consist of fibroblast-like cells, endothelial cells, nerve cells, preadipocytes, macrophages, and presumably other as yet unspecified cell types (3). The definition of obesity as a disease of chronic inflammation has recently come to prominence (9, 39, 44, 58). The contribution of adipose tissue adipocytes to this chronic inflammatory state is underscored by the now well-described secretory/endocrine function of adipose tissue. Adipocytes have been demonstrated to produce a range of local and/or systemic inflammatory mediators such as TNF- α and monocyte chemoattractant protein (MCP-1) and other factors (2, 19, 21, 25, 30, 47). Additionally, several lines of experimental data point to a very close phenotypic relationship between cells of the adipocyte lineage, i.e., preadipocytes and adipocytes, with macrophages (17, 22). Nonetheless, a somewhat unanticipated discovery was the magnitude to which obese WAT is subject to macrophage infiltration (1, 23, 25, 38, 56, 57, 59); it has been reported that such macrophages migrate from the bone marrow (56). Macrophages in adipose tissue are described to be in close proximity to apoptotic and/or dead adipocytes (20). Thus it is increasingly apparent that macrophages that are recruited to populate WAT play a key role in the type of chronic inflammatory state present in obesity (9, 15, 28, 39, 44, 45, 58). Importantly, interventions that decrease the degree of WAT macrophage infiltration may be effective at attenuating obesity-associated inflammation (8, 10, 14, 19, 25, 51).

In this study, we used the *ob/ob* genetically obese mouse model to identify gene expression distinctions between intra-abdominal epididymal (EP) and subcutaneous (SC) fat depots by construction and differential screening of a WAT-suppressive subtractive hybridization (SSH) cDNA library. We demonstrate that Slc37a2, a novel sugar transporter member of the major facilitator superfamily, evidences increased transcript expression in intra-abdominal EP vs. SC WAT depots. Furthermore, our findings indicate that among murine tissues, Slc37a2 transcript expression is restricted to the macrophage lineage and that this transcript evidences particularly enriched expression in *ob/ob* WAT. We propose that the Slc37a2 sugar transporter may perform a function that is integral to the metabolism of those macrophages that populate WAT in obesity.

METHODS AND PROCEDURES

RNA preparation and Northern blot analysis. RNA was purified using TRIzol reagent (Invitrogen, Carlsbad, CA) according to the

Address for reprint requests and other correspondence: C. M. Smas, Dept. of Biochemistry and Cancer Biology, Medical Univ. of Ohio, 3000 Arlington Ave., Toledo, OH 43614 (e-mail: csmas@meduohio.edu).

The costs of publication of this article were defrayed in part by the payment of page charges. The article must therefore be hereby marked “advertisement” in accordance with 18 U.S.C. Section 1734 solely to indicate this fact.

manufacturer's instructions. For studies of Slc37a2 transcript expression in murine tissues, 8-wk-old C57BL/6 or *ob/ob* male mice were utilized. All animal use was with the approval of the Medical University of Ohio Institutional Animal Care and Use Committee. For Northern blot analysis, 5 µg of RNA were fractionated in 1% agarose-formaldehyde gels in MOPS buffer and transferred to Hybond-N membrane (GE Healthcare, Piscataway, NJ). Blots were hybridized in ExpressHyb solution (BD Biosciences Clontech, Palo Alto, CA) for 1 h at 65°C with the indicated random primed ³²P-labeled cDNA probes. After being washed for 20 min at 65°C in 1% SDS/1× SSC and for 30 min at 65°C in 0.1% SDS/0.1× SSC, membranes were exposed at -80°C to Kodak BioMax film with a Kodak BioMax intensifying screen. For quantitative Northern blot assessments, the identical blot was hybridized with a probe for 36B4 transcript, which encodes the acidic ribosomal phosphoprotein PO, a commonly employed internal control (36). The ratio of the indicated transcript signal to that of 36B4 transcript for each sample was determined using a Typhoon 8600 PhosphorImager and ImageQuant software (GE Healthcare). Statistical analyses were conducted using single-factor ANOVA.

SSH cDNA library construction. To generate an *ob/ob* WAT depot subtractive library, the SSH method was used with WAT RNA prepared from 8-wk-old male *ob/ob* mice. SSH between intra-abdominal EP and SC WAT RNA was performed using the PCR-Select cDNA subtraction kit (BD Biosciences Clontech), according to the manufacturer's protocol. Tester cDNA was synthesized from total RNA of EP adipose tissue of *ob/ob* mice and driver cDNA from total RNA of SC adipose tissue of *ob/ob* mice. *Rsa*I-digested cDNA was purified with a NucleoTrap PCR kit (BD Biosciences Clontech). The tester cDNA was ligated with a cDNA adaptor provided by the manufacturer and hybridized with excess driver cDNA. After hybridization, differentially expressed transcripts were amplified by suppression PCR. Products from the nested PCR were gel-purified on 2% agarose gels and cDNA fragments were subcloned into pGEM-T vector (Promega, Madison, WI).

Differential screening of a WAT adipose depot SSH cDNA library. For array analysis, arrays contained 409 inserts of an SSH *ob/ob* WAT cDNA library. Filter arrays were prepared by PCR amplification of cDNA inserts directly from the arrayed bacterial stocks of the cDNA library using a nested primer set provided with the PCR-Select cDNA Subtraction kit. After denaturing the PCR products by incubation in 0.6 N NaOH, DNA was spotted onto Hybond-N⁺ nylon membranes (GE Healthcare) and membranes were neutralized by a 4-min incubation with 0.5 M Tris·HCl, pH 7.5, followed by fixation to the membrane by UV cross-linking. After prehybridization at 65°C for 1 h in 5 ml ExpressHyb solution containing 50 µl of 20× SSC and 50 µg of salmon sperm DNA, duplicate arrays were hybridized overnight at 65°C. Hybridization probes were reverse-transcribed ³²P-labeled cDNA populations synthesized from 8 µg of total RNA from *ob/ob* EP WAT and from *ob/ob* SC WAT depots. Posthybridization, filters were subjected to four incubations in low-stringency wash solution (2× SSC/0.5% SDS) at 65°C for 20 min each and two 20-min incubations in high-stringency wash solution (0.2× SSC/0.5% SDS) at 65°C and membranes were exposed at -80°C to Kodak BioMax film with a Kodak BioMax intensifying screen. cDNA clones of interest were subject to DNA sequencing and data were analyzed using NCBI GenBank databases and the BLAST algorithm.

Cell culture treatments and 3T3-L1 adipocyte differentiation. 3T3-L1 cells (American Type Culture Collection, Manassas, VA) were propagated in DMEM supplemented with 10% calf serum. For differentiation, 3T3-L1 cells were treated at 2 days postconfluence with DMEM supplemented with 10% FCS in the presence of the adipogenic inducers 0.5 mM methylisobutylxanthine and 1 µM dexamethasone for 48 h, as previously described (48). For treatment of 3T3-L1 adipocytes with TNF-α, cells were incubated with 10 ng/ml TNF-α for 16 h. For studies of regulation by insulin, 3T3-L1 adipocytes were first cultured for 16 h in serum-free DMEM with 0.5%

BSA. Cultures were then replenished with serum-free DMEM containing 0.5% BSA supplemented with 100 nM or 2 µM insulin for an additional 16 h. Murine macrophage RAW264.7 cells were cultured in DMEM supplemented with 10% FCS and THP-1 cells in RPMI media supplemented with 10% FCS, 10 mM HEPES, and 1 mM sodium pyruvate. For studies of the regulation of Slc37a2 transcript in RAW264.7 cells, near-confluent cell monolayers were treated for 24 h with 1 µM dexamethasone, 1 mM 8-bromo-dibutyryl cAMP, 10 ng/ml TNF-α, 100 mM sodium butyrate, 100 ng/ml LPS, 100 µM 9-*cis* retinoic acid, 200 µM indomethacin, or 10 nM triiodothyronine. Leptin treatment was at 500 ng/ml (Alexis Biochemicals, San Diego, CA) for 48 h. Unless otherwise stated, chemicals were from Sigma (St. Louis, MO). For leptin regulation of Slc37a2 transcript in RAW264.7 cells, methodology was as described below for human macrophage gene expression, using the following primers: Slc37a2 5'-TCACTTTAGTGCCAAGGAGG-3' and 5'-CAGCCAAGAT-CAGCATGATG-3', with correction against β-actin using primers 5'-TGGAACTCCTGTGGCATCCATGAAAC-3' and 5'-TAAACG-CAGCTCAGTAACAGTCCG-3'.

SLC37A2 transcript expression in human macrophage cell differentiation. For macrophage differentiation of THP-1 monocytes, cells were plated at 7 × 10⁶ per 100-mm culture dish and treated with 100 nM phorbol 12-myristate 13-acetate for 3 days. Total RNA was isolated using an RNeasy kit (Qiagen) with DNase I treatment (Qiagen) and reverse transcription was performed with SuperScript II RNase H-reverse transcriptase (Invitrogen) and an oligo(dT)-22 primer. Transcript levels of human SLC37A2, CD14, and GAPDH were assessed by SYBR green-based real-time PCR conducted with an ABI 7500 Real-Time PCR System (Applied Biosystems, Foster City, CA). Reaction conditions were 1× SYBR Green PCR Master Mix (Applied Biosystems), 100 nM each forward and reverse primers, and 50 ng of cDNA. PCR was carried out over 40 cycles of 95°C for 15 s, 60°C for 30 s, and 72°C for 34 s with an initial cycle of 50°C for 2 min and 95°C for 10 min. The following primers were used: SLC37A2, 5'-CACTTGCTGTGTCATGCTCATC-3' and 5'-TTGCCCTTCAGGCTC-TTGTC-3', CD14, 5'-AACTTCTCCGAACCTCAGCC-3' and 5'-TAG-GTCCTCGAGCGTCAGTT-3', and GAPDH, 5'-AACAGCCTCAAGAT-CATCAGC-3' and 5'-GGATGATGTTCTGGAGAGCC-3'. Expression of each gene was normalized against respective GAPDH transcript level and fold differences were calculated with the expression of SLC37A2 or CD14 present in untreated cells set to a value of 1. Three wholly independent experimental treatments were performed and statistical analyses were conducted using single-factor ANOVA.

Expression and localization of EGFP-Slc37a2 fusion protein. An EGFP-Slc37a2 expression construct was generated by PCR amplification of the complete coding sequence minus the initiator methionine using a 5' primer containing an *Xho*I site (underlined, 5'-TCATCTCGAGACGCTCCTCCCTGGCTCCTGG-3') and 3' primer containing an *Sal*I site (underlined, 5'-GGCAGTTCGACT-CAAATTTGTTTGTACCCACTGCTTC-3'). PCR amplicons were cloned into pCR2.1-TOPO vector and the insert was transferred into pEGFP-C3 vector (BD Biosciences Clontech). The PCR-amplified Slc37a2 portion of this expression construct and the cloning junctions were fully sequenced. For EGFP detection in live cells, COS cells were transfected with either the EGFP-Slc37a2 expression construct or empty EGFP vector using Lipofectamine 2000 (Invitrogen) and assessed at 48 h posttransfection. For studies with Texas Red dextran, COS cells were transfected as above and at 24 h posttransfection cells were washed twice with phenol-red free DMEM/10% FCS and incubated for 16 h in phenol-red free DMEM/10% FCS supplemented with 0.5 mg/ml 10,000 M_r Texas Red dextran (Invitrogen). Following incubation, cells were washed twice with phenol-red free DMEM/10% FCS and incubated an additional 2 h in phenol-red free DMEM/10% FCS. For studies with organelle-specific tracking probes (Invitrogen), MitoTracker Red CMX ROS, LysoTracker Red DND-99, ER-Tracker Blue-White DPX, and BODIPY Texas Red C5-ceramide complexed to BSA for Golgi detection were for used for staining live

cells based on manufacturer's guidelines. Cells were observed using an Olympus IX70 microscope and digital images were obtained and merged using Spot Advanced software (Diagnostic Instruments, Sterling Heights, MI).

Slc37a2 expression constructs and Western blot analysis. An expression construct for Slc37a2 that contained a COOH-terminal HA tag was generated by PCR amplification of the complete coding sequence for Slc37a2 using a mouse I.M.A.G.E. clone (GenBank accession number BC063326) as template. For this, a 5' PCR primer (5'-TCA-TCTCGAGATGCGGTCCTCCCTGGCTCTGG-3') was used in combination with a 3' primer that incorporated a COOH-terminal HA tag followed by a stop codon (5'-GGCAGTCTCGACTCAAAGAGCGTAATCTGGAACATCGTATGGGTAAATTTGTTGTACCACTGCTTC-3') with an *Xho*I site (underlined) and a *Sal*I site (underlined), respectively. PCR product was cloned into the pCR2.1-TOPO vector (Invitrogen) and insert was transferred into pcDNA3.1 vector (Invitrogen). The PCR-amplified Slc37a2 portion of this expression construct and the cloning junctions were fully sequenced. For Western blot analysis, cell lysate was prepared by harvest in lysis buffer (50 mM Tris·HCl, pH 8.0, 150 mM NaCl, 1% NP-40, and 200 μM PMSF) and following removal of insoluble matter protein concentration was determined. Samples were fractionated on 8% SDS-PAGE and electroblotted onto PVDF membrane with 0.025 M Tris/0.192 M glycine transfer buffer containing 10% methanol. Following transfer, membranes were blocked in 5% nonfat milk in PBS/0.5% Tween 20 (PBS-T) for 1 h and incubated with monoclonal anti-HA antibody (cat. no. MMS-101R, Covance, Berkeley, CA) at a 1:4,000 dilution for 1 h and horseradish peroxidase-conjugated goat anti-mouse (cat. no. SC-2005, Santa Cruz Biotechnology, Santa Cruz, CA) at a 1:2,000 dilution for 30 min. All washing of Western blots was conducted in PBS-T. After the final wash, signals were detected by incubation in ECL plus reagent (GE Healthcare) and exposure to Fuji RX film.

Analysis of Slc37a2 protein glycosylation. COS or HeLa cells were transiently transfected with HA-tagged Slc37a2 expression construct or empty vector using Lipofectamine 2000. For PNGase F digestion, cell lysates of transfected HeLa cells were boiled in denaturing buffer (0.5% SDS/0.04 M DTT) for 10 min and the sample was adjusted to 1% Nonidet P-40, 50 mM sodium phosphate, pH 7.5, and 45 U/ml PNGase F (New England BioLabs, Beverly, MA) and supplemented with a protease inhibitor cocktail (Sigma). Sample was incubated for 1 h at 37°C followed by 8% SDS-PAGE and Western blot analysis was carried out with an anti-HA antibody as described above. Neuraminidase digestion was performed using *V. cholerae* neuraminidase (Sigma) as described previously (48). In vitro transcription and translation of HA-tagged Slc37a2 were performed with a TNT T7 Quick Coupled Transcription/Translation System (Promega). After a 1.5-h incubation at 30°C, 1 μl of the reactions was analyzed by Western blot. For tunicamycin treatment, at 6 h posttransfection cells were incubated in the presence of 1 mg/ml tunicamycin (Alexis Biochemicals) or DMSO vehicle, and protein was harvested 16 h.

Site-directed mutagenesis of consensus N-linked glycosylation sites was carried out employing the HA-tagged Slc37a2 expression construct as template and using a GeneEditor in vitro Site-Directed Mutagenesis System (Promega). The asparagine of the respective N-linked consensus site was mutated to alanine using the following primers: for the N53 site, 5'-CCGCTGCACCAGGCCTGCTCAGAGAT GG-3'; for the N62 site, 5'-TGGTCAGAC CTGTTGCTGACACCCACGATC-3'; and for the N68 site, 5'-ACACCCACGATCTCG CTGATACCACCTGGT G-3'. Mutations were confirmed by DNA sequencing.

RESULTS

Subtractive screening identifies Slc37a2 as a WAT depot-enriched transcript. To identify transcripts that show increased expression in the EP WAT depot, we utilized the SSH method and prepared a subtracted cDNA library by subtracting tran-

scripts present in *ob/ob* SC WAT from *ob/ob* EP WAT. cDNA clones of this SSH cDNA library were arrayed onto replicate nylon membranes and hybridized with reverse-transcribed probes generated from *ob/ob* SC or *ob/ob* EP WAT depot total RNA, and differential signals were visually assessed. Of the 409 clones screened, 237 evidenced approximately twofold or greater enriched expression in *ob/ob* EP WAT vs. *ob/ob* SC WAT. Figure 1A shows an example of a portion of the replicate membranes screened in this manner. The arrows indicate one of the transcripts, Slc37a2, noted to show higher expression level in the EP vs. SC WAT depot. A number of putative differentially expressed clones were sequenced and several of these were used to validate expression level in SC and EP WAT of two individual *ob/ob* mice. As presented in Fig. 1B, Northern blot analyses of RNA from SC and EP *ob/ob* WAT depots indicate differential upregulation of transcripts for Slc37a2, ferritin light chain, prosaposin, cathepsin S, and cathepsin H in the EP WAT depot.

We focused our attention on one of these differentially expressed transcripts, Slc37a2. This was due to the degree of differential expression we noted in Fig. 1B and the nature of the encoded protein as a putative sugar transporter of unspecified function; the latter raising the possibility of a role in energy metabolism. There has been little study of the Slc37a2 gene product. The single publication to date describes the cloning of this cDNA, among a number of others, during a differential display screening for genes upregulated by 8-bromodibutyryl-cAMP in murine RAW264.7 macrophages; its transcript expression was also detected in bone marrow-derived mouse macrophages (49). Slc37a2, along with Slc37a1, Slc37a3, and Slc37a4, comprises the four members of the Slc37a sugar transporter family (5). The murine Slc37a2 protein consists of 510 amino acids of a calculated molecular mass of 55,059. Our sequence analysis and hydropathy predictions for Slc37a2 indicate it possesses 12 transmembrane domains and is a member of the major facilitator superfamily (MFS). MFS proteins are typically 12 transmembrane pass, single polypeptide encoded, secondary carriers that transport solutes in response to electrochemical gradients and include uniporter, symporter, and antiporter functional classes (41). The protein sequence of Slc37a2 is shown in Fig. 2A with the 12 predicted transmembrane domains designated by underlining and the hydropathy plot for Slc37a2 protein is shown in Fig. 2B. Within the MFS, the sugar transporter subfamily is the largest subcategory with GLUT1 as the prototypical member (4). A defining characteristic of the GLUT-type sugar transporters is the presence of two G-R-K/R motifs, one between transmembrane helices 2 and 3 and the second between helices 8 and 9. Slc37a2 does not contain this signature motif, or recognizable variations thereof, nor does it possess overall homology to GLUT-type transporters. Thus it is unlikely to be a GLUT type sugar transporter but to be of a novel type. Analysis with the NCBI Conserved Domain database indicates that Slc37a2 evidences the highest degree of homology to the UhpC sugar permease domain. Proteins of this type are involved in uptake of a number of sugar phosphates or other phosphorylated metabolites. To our knowledge, no functional assessment of transporter activity or substrate specificity has been described for mammalian Slc37a2 or for this protein in any other species. The NCBI GenBank annotation classifies it as a glycerol 3-phosphate transporter, likely based on its homology

with bacterial sugar transporters, particularly *Escherichia coli* GlpT (31, 37), a glycerol 3-phosphate permease. Those amino acids that are identical for murine Slc37a2 and *E. coli* GlpT are indicated by bold italic typeface in Fig. 2A.

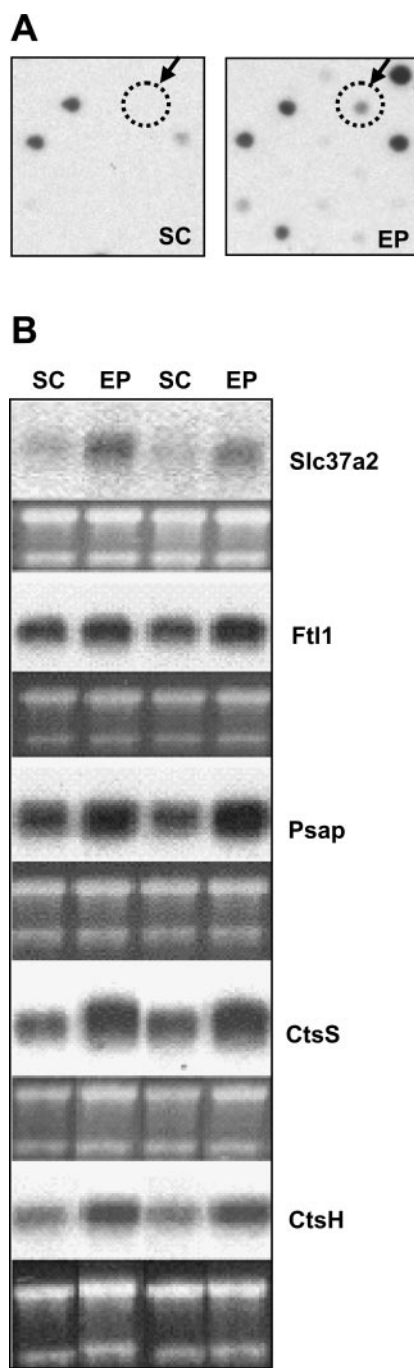


Fig. 1. Differential expression of Slc37a2 transcript in white adipose tissue (WAT) depots. *A*: suppressive subtractive hybridization (SSH) library was differentially screened with ^{32}P -labeled reverse-transcribed probes generated from total RNA of either *ob/ob* subcutaneous (SC) or *ob/ob* epididymal (EP) WAT. The arrow and dashed circle indicate position of Slc37a2 signal on the dot blot. *B*: Northern blots for differentially expressed transcripts in *ob/ob* SC or *ob/ob* EP WAT depots using random-primed ^{32}P -labeled probes for Slc37a2, ferritin light chain 1 (Ftl1), prosaposin (Psap), cathepsin S (CtsS), and cathepsin H (CtsH). The EtBr staining of rRNA is shown below the respective autoradiogram.

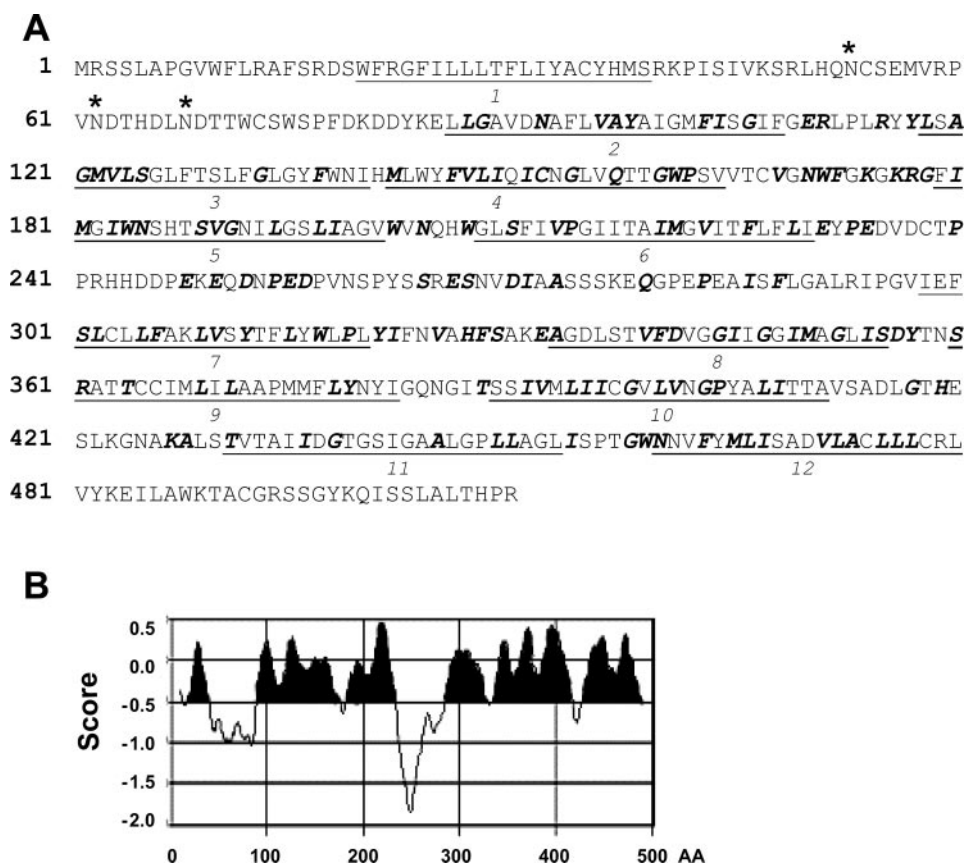
Database analysis reveals the Slc37a2 gene is present in both vertebrate and invertebrate genomes with homologs found in human, dog, chick, plants, fly, zebrafish, and other species. Analysis of the Slc37a2 protein sequence reveals the presence of three consensus sites for N-linked glycosylation (N-X-S/T, X \neq P) present between predicted transmembrane regions 1 and 2. As discussed by Bartoloni and Antonarakis (5), the four Slc37a proteins share a moderate degree of protein sequence homology. Our database analysis indicates that over their respective full protein sequences, Slc37a2 and Slc37a1 evidence $\sim 60\%$ identity and Slc37a2 and Slc37a3 evidence $\sim 40\%$ identity. Slc37a2 and Slc37a4 have $\sim 20\%$ identity; however, this is found only in regard to the NH₂-terminal halves of the two proteins.

Depot enrichment of Slc37a2 transcript is attributable to differential macrophage infiltration of intra-abdominal WAT. Since Slc37a2 transcript was present in WAT, we next examined whether expression of Slc37a2 could be detected in a well-established model of in vitro adipocyte differentiation, murine 3T3-L1 cells. Hybridization with the adipocyte marker genes stearoyl co-A desaturase 1 (SCD1) and adipocyte fatty acid binding protein (aFABP), shown in Fig. 3A, indicates effective in vitro adipocyte conversion of 3T3-L1 preadipocytes. Figure 3A reveals that the Slc37a2 transcript is not detected in either 3T3-L1 preadipocytes or adipocytes, with EP WAT of *ob/ob* mice included for comparison (Fig. 3A, last lane). In addition, neither treatment with TNF- α nor insulin, two agents key in modulating adipocyte gene expression and physiology, resulted in detectable levels of Slc37a2 transcript in 3T3-L1 adipocytes.

We next addressed whether Slc37a2 transcript level in *ob/ob* WAT would specifically track with the presence of macrophages by using expression of the robust macrophage-specific marker *emr1* (33), also known as F4/80. As shown in Fig. 3B, *emr1* transcript level tracks closely with that for Slc37a2 in *ob/ob* WAT with a similar pattern of Slc37a2 and *emr1* signal intensity seen across the SC, EP, and retroperitoneal (RP) WAT depots, and nearly lack of detection of either transcript in brown adipose tissue (BAT). The high expression in RP WAT, a distinct type of intra-abdominal WAT depot, supports our finding of differential expression of Slc37a2 in intra-abdominal (i.e., EP and RP) WAT vs. SC WAT. Also shown in this figure is the level of Slc37a2 in RAW264.7 macrophages. In contrast, the well-characterized adipocyte marker transcripts SCD1 and aFABP are expressed at a similar level across the three WAT depots and are also readily detected in BAT. Together, these data lead to the conclusion that macrophages present in *ob/ob* WAT are likely the major cell type responsible for the WAT expression of Slc37a2 transcript.

We next conducted studies to more precisely assess whether the difference in magnitude of expression of the Slc37a2 transcript we find between SC and EP *ob/ob* WAT depots could be explained solely by the differential presence of tissue macrophages in these two WAT depots. For this, we conducted quantitative Northern blot analysis for Slc37a2 and *emr1* transcripts for SC and EP WAT depots for four individual *ob/ob* mice. A statistically significant increase of approximately two-fold is noted for Slc37a2 (Fig. 3C) and *emr1* (Fig. 3D) transcripts. Graphical representation of the ratio of Slc37a2 to *emr1* transcript level is shown in Fig. 3E. Here, we find that the Slc37a2 to *emr1* transcript ratio is similar for the SC and the EP

Fig. 2. Amino acid sequence of the major facilitator superfamily protein Slc37a2. A: predicted amino acid sequence of murine Slc37a2. The numbers at left indicate amino acid positions. The 12 transmembrane domains are underlined and numbered designated based on protein topology predictions utilizing the TMHMM server version 2.0. The 3 putative N-glycosylation sites at positions 53, 62, and 68 are designated with *. Those amino acids showing identity with the *E. coli* protein GlpT are depicted in bold italic typeface. B: hydropathy analysis of Slc37a2 protein sequence. Slc37a2 protein sequence was subject to the von Heijne algorithm using DS Gene 2.1 software, with a window size of 21. Filled areas indicate each of the 12 predicted transmembrane domains. The hydropathy score is shown on the y-axis and the amino acid (AA) number on the x-axis.



WAT depot. We interpret this to indicate that an enrichment of adipose tissue macrophages in the EP depot likely accounts for the upregulation of Slc37a2 transcript we observe between EP vs. SC *ob/ob* WAT depots.

Slc37a2 shows marked enrichment in *ob/ob* WAT. Given the degree of enrichment of macrophages reported for obese WAT (9, 15, 28, 39, 44, 45, 58), if adipose tissue macrophages were indeed responsible for WAT Slc37a2 transcript expression, it would be predicted to evidence enriched expression in obese vs. wild-type WAT. We therefore quantitatively compared Slc37a2 and *emr1* transcript levels, and their relative ratios, in wild-type SC vs. *ob/ob* SC WAT and in wild-type EP vs. *ob/ob* EP WAT, shown in Fig. 4, left and right columns, respectively. The Northern blot of the data for SC WAT is shown in Fig. 4A and indicates marked enrichment of Slc37a2 and *emr1* transcripts in *ob/ob* SC WAT. Figure 4B illustrates that a statistically significant increase of sevenfold is noted for the level of Slc37a2 transcript in *ob/ob* SC WAT compared with wild-type, while the *emr1* transcript level is enriched by about twofold (Fig. 4C). In contrast to the approximately ninefold difference noted for the Slc37a2 transcript, wild-type SC and *ob/ob* SC WAT express similar levels of two adipocyte marker transcripts, aFABP and SCD1. Given that *emr1* is a highly specific macrophage marker, the twofold increase in *emr1* transcript level in *ob/ob* vs. wild-type SC WAT likely reflects macrophage infiltration in obese tissues, consistent with recent reports (9, 39, 56, 58). Figure 4D illustrates that the Slc37a2 to *emr1* transcript ratio is ~ 4.5 ; this suggests that Slc37a2 transcript level may be upregulated in that population of macrophages that infiltrate obese adipose tissue. As shown by the

Northern blot (Fig. 4E), data for Slc37a2 transcript expression in wild-type EP vs. *ob/ob* EP WAT are similar to that found for SC WAT; namely, an approximately ninefold enrichment of Slc37a2 transcript level (Fig. 4F), an approximately twofold enrichment for *emr1* transcript (Fig. 4G), and a Slc37a2 to *emr1* transcript level ratio of ~ 4.5 for wild-type vs. *ob/ob* EP depots (Fig. 4H). The differential *emr1* transcript expression we show here in obese WAT also serves as independent evidence of macrophage infiltration into WAT in obesity and highlights the utility of the murine *ob/ob* obesity model for studies on the mechanisms of this infiltration.

Slc37a2 transcript expression in murine tissues and macrophages. To further investigate Slc37a2 transcript expression pattern(s), we conducted Northern blot analysis on a panel of murine tissues. For wild-type mice (Fig. 5A) Slc37a2 transcript is restricted to two tissue types rich in macrophages, spleen and thymus; its expression had previously been reported to be readily detected in bone marrow-derived murine macrophages (49). Among *ob/ob* tissues, Fig. 5B, we find that it is the EP WAT sample that evidences highest transcript expression. We also note that the apparent Slc37a2 to *emr1* transcript level ratio is distinct in spleen vs. WAT. A higher relative expression level of Slc37a2 to *emr1* transcript level is noted in WAT, possibly indicating that the macrophages present in *ob/ob* WAT are enriched for Slc37a2 transcript, compared with splenic macrophages.

To begin to address the nature of expression and regulation of the Slc37a2 transcript in macrophages, we treated murine RAW264.7 macrophages with a number of agents and assessed Slc37a2 transcript level by Northern blot (Fig. 6A). Here, we

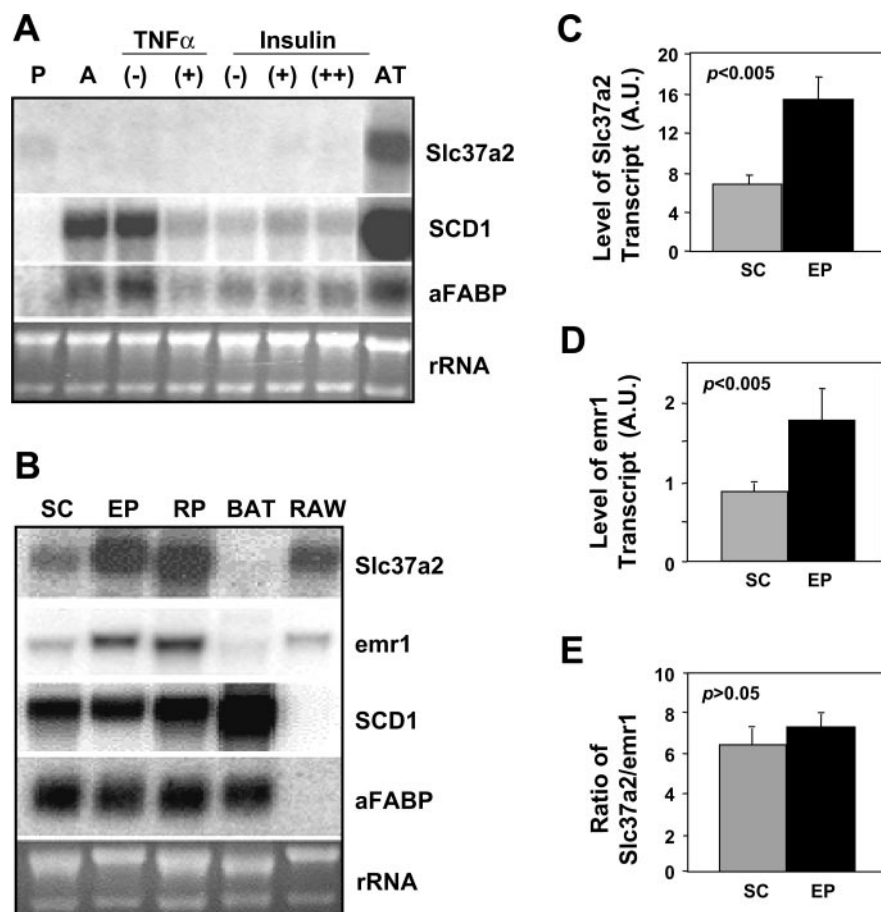


Fig. 3. Assessment of expression of Slc37a2 and/or emr1 transcript in adipocytes and WAT depots. **A:** total RNA was prepared from 3T3-L1 preadipocytes (P), 3T3-L1 adipocytes (A), and 3T3-L1 adipocytes treated with 10 ng/ml of TNF- α , 100 nM (+) or 2 μ M (++) insulin for 16 h. For a positive control, *ob/ob* EP WAT (AT) is in the rightmost lane. Slc37a2, SCD1, and aFABP transcript expression was analyzed by Northern blot using 32 P-labeled reverse transcribed probes. **B:** expression of Slc37a2 transcript in adipose tissues. Five micrograms of total RNA from SC, EP, retroperitoneal (RP) WAT, and brown adipose tissue (BAT) of *ob/ob* mice and that of RAW264.7 murine macrophages (RAW) were analyzed by Northern blot using 32 P-labeled probes for Slc37a2, emr1, SCD1, and aFABP. For A and B, the EtBr staining of rRNA is shown below the respective autoradiogram. **C:** quantitation of Slc37a2 transcript expression level in SC and EP adipose tissues of 4 *ob/ob* mice. **D:** quantitation of emr1 transcript expression level in SC and EP adipose tissues of 4 *ob/ob*. **E:** ratio of Slc37a2 and emr1 was calculated based on transcript expression level of Slc37a2 (in C) and emr1 (in D). Data were collected via phosphorimager quantitation and each expression was corrected against its 36B4 control. Data represent means \pm SD analyzed by single-factor ANOVA ($n = 4$).

find that, as previously described, exposure to 8-bromo dibutyryl cAMP upregulates Slc37a2 transcript (49). Of the other agents tested, only sodium butyrate, a short-chain fatty acid that possesses histone deacetyltransferase-inhibiting activity, affected Slc37a2 transcript level, with an 85% decrease observed. None of the other agents tested, including those integral to macrophage function, such as TNF- α and LPS, or leptin (data not shown) led to an alteration of the level of endogenous Slc37a2 transcript.

We next examined expression of SLC37A2 transcript in human macrophages using THP-1 cells (Fig. 6B). Upon treatment with phorbol 12-myristate 13-acetate, THP-1 cells undergo macrophage differentiation as evidenced by adherence and spreading on culture dishes and by upregulation of genes indicative of macrophage differentiation. As expected, the level of expression of the macrophage marker transcript CD14 is dramatically induced as a result of the differentiation protocol (Fig. 6B, left). Strikingly, we observed a 46-fold increase in expression level of SLC37A2 transcript upon macrophage differentiation of THP-1 cells (Fig. 6B, right). We have also observed a similar magnitude of increase for SLC37A2 transcript upon macrophage conversion of HL-60 cells (data not shown). These data reveal that SLC37A2 transcript is expressed in human macrophage cells and, moreover, its upregulation appears to be closely tied to emergence of the macrophage phenotype.

Ectopic expression of Slc37a2 results in the appearance of large intracellular vacuoles. To investigate the subcellular localization of Slc37a2, we utilized an EGFP-Slc37a2 fusion protein construct and carried out studies using transfected COS cells. The results of these studies (Fig. 7A) indicate that expression of Slc37a2 results in the accumulation of large intracellular vacuoles that are clearly rimmed with signal for the EGFP-Slc37a2 fusion protein. Oil Red O staining for lipid indicated that the vacuoles do not contain lipid (data not shown). To determine whether the vacuoles might arise from endocytosis of the plasma membrane, we incubated EGFP-Slc37a2 or empty vector-transfected COS cells in media supplemented with 10,000 M, Texas Red dextran. Shown in Fig. 7B, a subpopulation of these vacuoles clearly contains well-defined circular regions of Texas Red signal that colocalize with the vacuoles. In contrast, a more diffuse appearance of Texas Red signal is found in cells lacking EGFP-Slc37a2 signal, typified by the cell indicated to the left of the field, designated by the arrow. In an attempt to define the subcellular origin of the vacuoles, we utilized a number of molecular probes for intracellular organelles (Invitrogen). Neither trackers for mitochondria, endoplasmic reticulum, Golgi apparatus, nor lysosomes yielded signals that colocalized with that for EGFP-Slc37a2 (data not shown).

Analysis of Slc37a2 protein reveals heterogeneity of mass and N-linked sugars. To begin studies on the fundamental nature of the Slc37a2 protein, we first used in vitro transcrip-

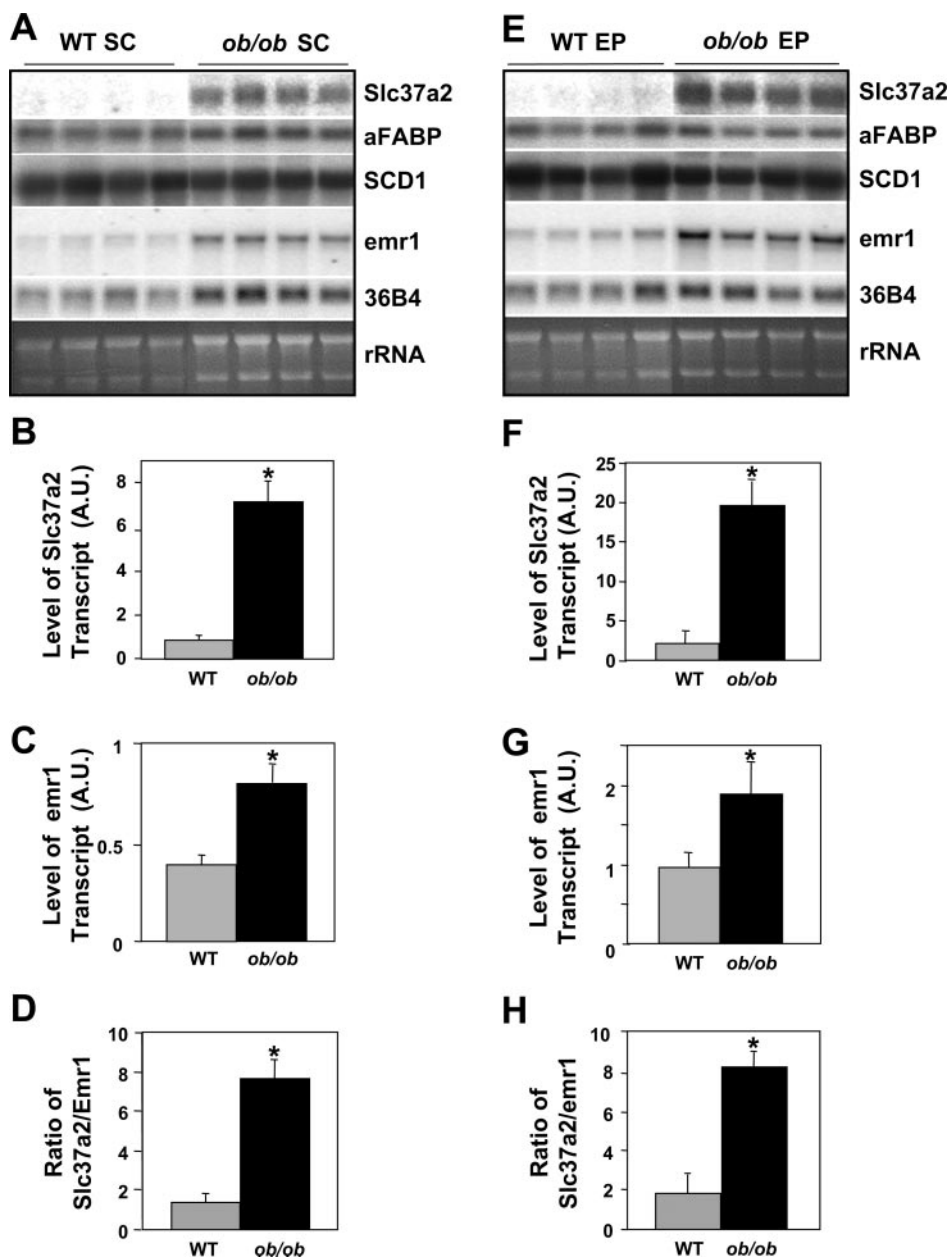


Fig. 4. Expression of Slc37a2, emr1, and select adipocyte transcripts in wild-type (WT) vs. *ob/ob* WAT depots. **A**: Northern blot analysis of 5 μ g of total RNA from the SC adipose tissue of 4 individual WT or 4 individual *ob/ob* mice. Hybridization was conducted using 32 P-labeled random-primed probes for Slc37a2, aFABP, SCD1, emr1, and 36B4. The EtBr staining of rRNA is shown below the respective autoradiogram. **B–D**: quantitation of Northern blot data in **A** corrected against expression of 36B4 internal control, showing the relative transcript expression level for Slc37a2 (in **B**) and emr1 (in **C**), with the ratio of Slc37a2 and emr1 plotted in **D**. **E**: Northern blot analysis of 5 μ g of total RNA from the EP adipose tissue of 4 individual WT or 4 individual *ob/ob* mice. Hybridization was conducted using 32 P-labeled random-primed probes for Slc37a2, aFABP, SCD1, emr1, and 36B4. The EtBr staining of rRNA is shown below the respective autoradiogram. **F** and **G**: quantitation of the Northern blot data in **E** corrected against expression level for the 36B4 internal control, showing the relative transcript expression level for Slc37a2 (in **F**) and emr1 (in **G**), with the ratio of Slc37a2 and emr1 plotted in **H**. Data were collected via phosphorimager quantitation and represent means \pm SD analyzed by single-factor ANOVA ($n = 4$) and $*P < 0.005$ for *ob/ob* vs. WT.

tion and in vitro translation of the open reading frame of Slc37a2 fused to a COOH-terminal HA tag to investigate the size of the primary translation product. Western blot analysis using HA antibody, shown in Fig. 8A, reveals that the primary translation product of Slc37a2 migrates at ~ 50 kDa, in good agreement with the size predicted from its open reading frame. To examine the nature of the Slc37a2 protein expressed in mammalian cells, we utilized transient transfection of HA-tagged Slc37a2 expression construct or an empty vector negative control plasmid. Figure 8, B and C, for HeLa and COS cells, respectively, shows that the Slc37a2 protein appears as a poorly resolved heterogeneous species with the most intense signal(s) found from 50 to 75 kDa.

We next asked whether the discrepancy between the in vitro translation product of ~ 50 kDa and the heterogeneous signal present in transfected cells was due to posttranslational addi-

tion of N-linked and/or O-linked sugars. As was presented in Fig. 2A, three N-linked glycosylation sites are noted in Slc37a2, located between the first and second predicted transmembrane domains. Cell lysates were prepared from HeLa cells transfected with HA-tagged Slc37a2 expression construct or empty vector. Lysates were incubated with the enzyme PNGase F to digest N-glycans or incubated under mock conditions and processed for Western blot with the HA antibody. Figure 8D reveals that PNGase F treatment led to a marked decrease in Slc37a2 protein mass and the appearance of a more distinct signal of ~ 50 kDa. These data indicate that Slc37a2 is modified via the addition of N-linked sugar groups. This conclusion is also supported by the Western blot data in Fig. 8E. For this, the HA-tagged Slc37a2 expression construct was transfected into COS cells and cells subjected to culture in the absence or presence of tunicamycin, an inhibitor of N-

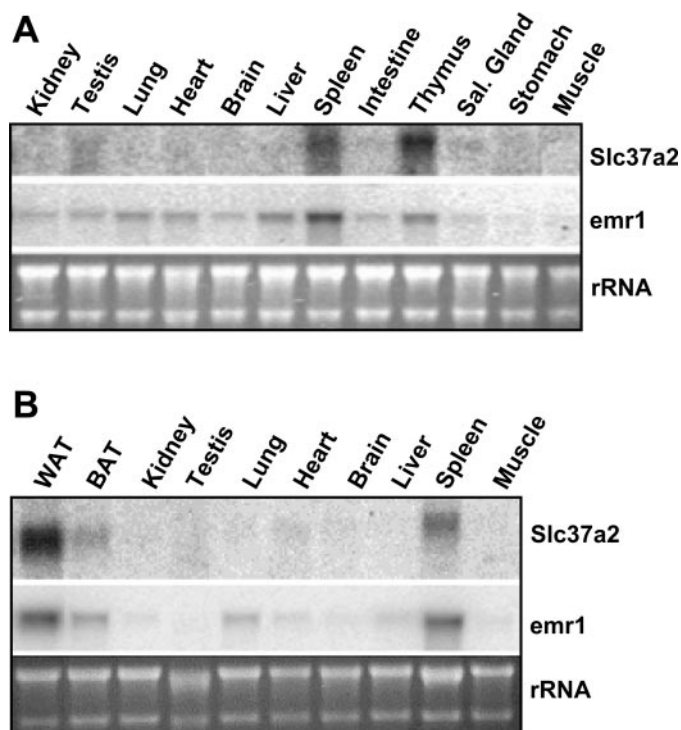


Fig. 5. Tissue-specific expression pattern of Slc37a2 transcript in a panel of wild-type and *ob/ob* murine tissues. Five micrograms of total RNA from indicated wild-type mouse tissues (A) and *ob/ob* mouse tissues (B) were analyzed by Northern blot using ^{32}P -labeled murine Slc37a2 and *emr1* probes. Sal, salivary. For A and B, the EtBr staining of rRNA is shown below the respective autoradiogram.

linked glycosylation. Here, tunicamycin treatment results in a decrease in the mass and heterogeneity of the Slc37a2 protein, to a size consistent with that of the *in vitro* translation product. We do not presently know the origin or identity of the smaller species of the Slc37a2-HA fusion protein present in the PNGase F and tunicamycin-treated samples. Western blot analysis for cell lysates prepared from HeLa cells transfected with the HA-tagged Slc37a2 expression construct and treated with *V. cholera* neuraminidase showed no alteration in the appearance of Slc37a2 protein, indicating it does not evidence posttranslational modification by O-linked sugars (data not shown). To assess the contribution of each of the three putative N-linked glycosylation sites to the heterogeneity of the Slc37a2 protein, we conducted site-directed mutagenesis to alter each to alanine. These mutations did not appreciably affect the size or degree of heterogeneity observed for the Slc37a2 protein (data not shown). This suggests that it is not a single one of the three putative N-linked glycosylation sites that contributes to Slc37a2 glycosylation but is rather a combinatorial effect.

DISCUSSION

Our data reveal that Slc37a2 is a new macrophage-specific transcript that we predict to play a transport role in macrophage metabolism. The structural motifs of Slc37a2 clearly place it in the MFS as a putative sugar transporter; however, the substance(s) transported by this Slc37a2 and their role in macrophage function remain to be determined. Of the four Slc37a proteins, only Slc37a4, also known as the microsomal glucose-

6-phosphate translocase 1 (G6PT1), has been studied in detail and has been empirically demonstrated to possess transporter function (18). Defects in Slc37a4/G6PT1 are responsible for glycogen storage disease type Ib (GSD-Ib) (26, 43). GSD-Ib patients show disrupted glucose homeostasis and immune system complications of intermittent neutropenia and defects in neutrophil respiratory burst and chemotaxis (18, 40). Given the demonstrated function of Slc37a4 in the immune system, it is noteworthy that we have now found Slc37a2 to be specifically expressed in a cell type of the immune system, i.e., the macrophage. It is possible that similar to Slc37a4, Slc37a2 is key to aspects of immune system function(s). Data on the Slc37a1 and Slc37a3 genes/proteins are surprisingly scant and limited to transcript expression. Slc37a1 transcript has been reported in adult bone marrow, colon, small intestine, kidney, liver, and other tissues, with particularly enriched expression noted in tissues evidencing a high rate of gluconeogenesis (5, 6). Given its homology to the *E. coli* glycerol 3-phosphate permease GlpT (37), Slc37a1 is presumed to be a glycerol 3-phosphate transporter that would function by exchanging glycerol 3-phosphate and inorganic phosphate (5, 6). Expression data on Slc37a3 are limited to *in silico* assessment of EST cDNA clone frequencies where it appears to be particularly enriched in cDNA libraries derived from breast and stomach (5).

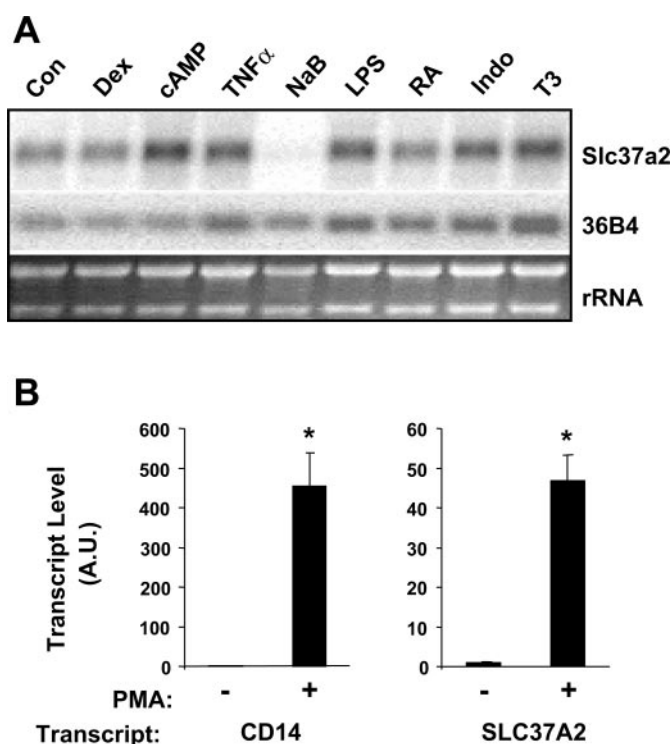


Fig. 6. Expression and regulation of Slc37a2 transcript in macrophages. A: RAW264.7 macrophages were treated with the indicated agents for 24 h and 5 μg of total RNA were subject to Northern blot analysis using ^{32}P -labeled probe for Slc37a2 and 36B4. The EtBr staining of rRNA is shown below the autoradiogram. Con, control; Dex, dexamethasone; NaB, sodium butyrate; RA, 9-*cis* retinoic acid; Indo, indomethacin; T3, triiodotyronine. B: expression of SLC37A2 transcript in human macrophage differentiation. THP-1 cells were untreated (-) or treated (+) for 3 days with phorbol 12-myristate 13-acetate (PMA) and the relative transcript level of CD14 (left) and SLC37A2 (right) was determined by real-time PCR. Data represent means \pm SD for 3 independently conducted experiments and were analyzed by single-factor ANOVA with $*P < 0.001$ for treated (+) vs. untreated (-) cultures.

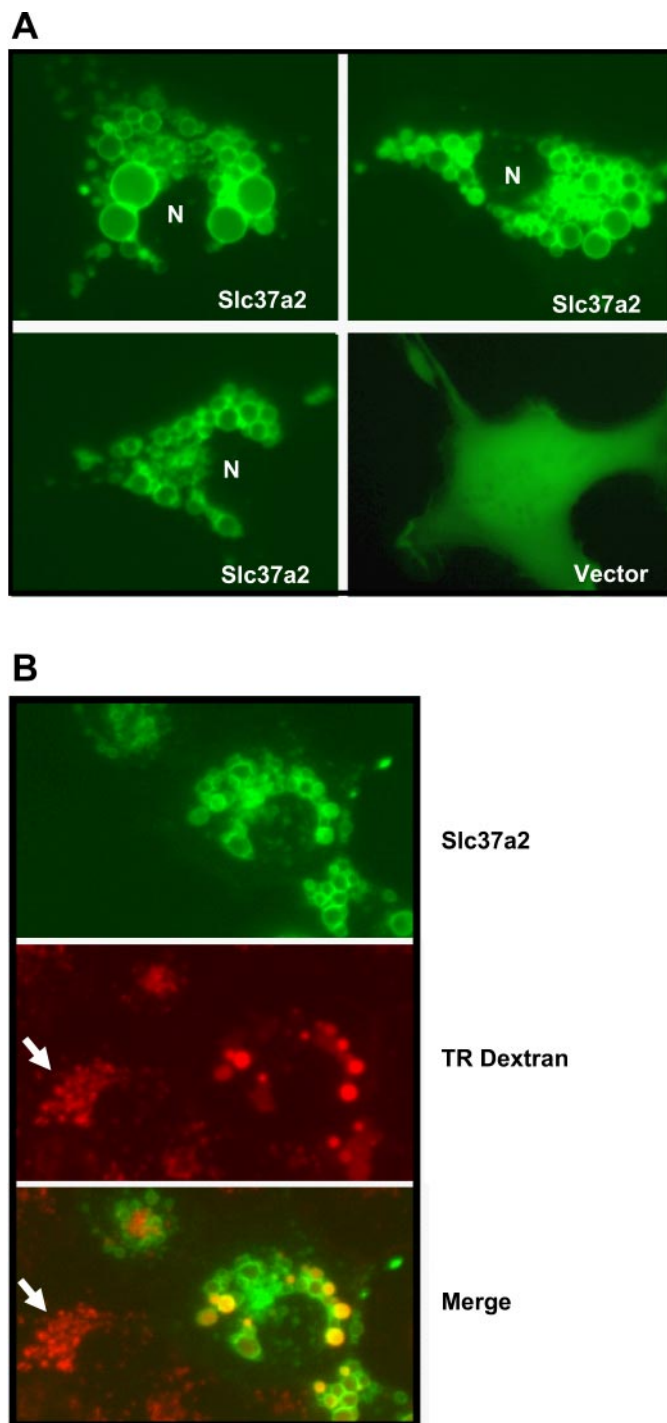


Fig. 7. Slc37a2 protein expression induces formation of Texas Red dextran-positive intracellular vacuoles. *A*: expression of EGFP-Slc37a2 fusion protein in COS cells. Cells were transfected with an EGFP-Slc37a2 expression construct (Slc37a2, 3 panels shown) or empty EGFP vector (Vector, 1 panel shown) and visualized for EGFP at 48 h posttransfection. The location of the nucleus (N) is indicated. *B*: uptake of Texas Red dextran into Slc37a2-induced vacuoles. Cells were transfected, as in *A*, and during the final 16 h of a 48-h posttransfection culture period, cells were incubated in the presence of 10,000 M_r Texas Red dextran. *Top*: EGFP signal. *Middle*: Texas Red (TR) dextran signal. *Bottom*: merged image. Arrow indicates a nontransfected cell with diffuse Texas Red signal, as noted in the text.

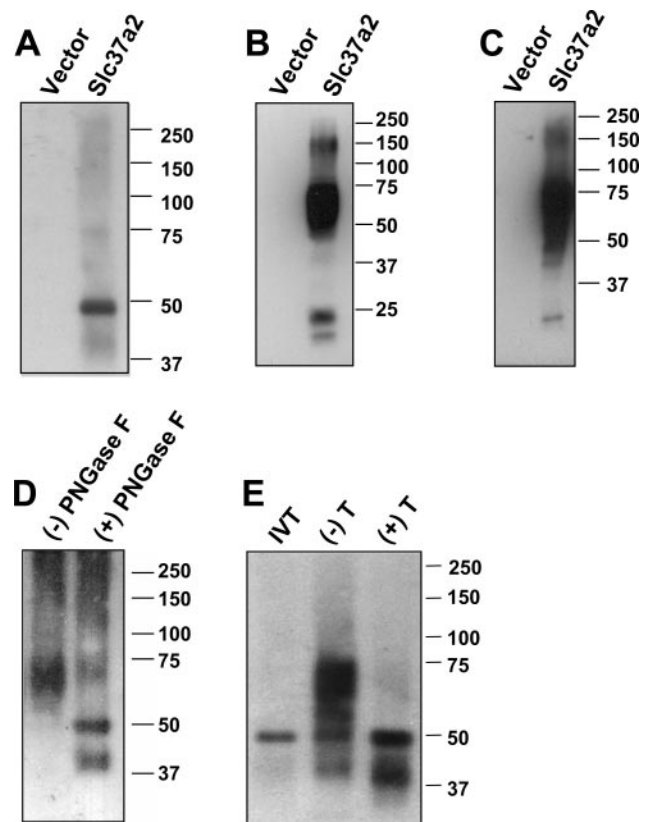


Fig. 8. Slc37a2 is subject to N-linked glycosylation to result in protein size heterogeneity of 50–75 kDa. *A*: Western blot analysis of HA-tagged Slc37a2 in vitro translation product. *B*: HeLa cells were transfected with HA-tagged Slc37a2 expression construct or empty vector and Western blot analysis was performed using HA antibody. *C*: COS cells were transfected with HA-tagged Slc37a2 expression construct or empty vector and Western blot analysis was performed using HA antibody. *D*: HA-tagged Slc37a2 expression construct was transfected into HeLa cells and cell lysates collected at 48 h posttransfection. Lysates were incubated in the absence (–) or presence (+) of PNGase F followed by Western blot analysis performed with HA antibody. *E*: HA-tagged Slc37a2 expression construct was transfected into COS cells and 6 h posttransfection cells were subject to a 16-h incubation in the absence (–) or presence (+) of tunicamycin (T). Cell lysates were assessed for HA-tag by Western blot. For comparison purposes, the first lane contains the result of an in vitro translation reaction (IVT), as in *A*.

The nature of the vacuoles observed on ectopic expression of the Slc37a2 protein is currently unclear. However, the observation that a subset of these vacuoles were positive for Texas Red dextran signal suggests that either the vacuoles are directly involved in uptake from the extracellular environment or, on the other hand, that they are intracellular in nature but undergo fusion with endocytic vacuoles to result in the appearance of Texas Red dextran in their interior. Vacuoles of a similar appearance have been noted on ectopic expression of the chloride-iodide transporter protein pendrin in cultured cells. This phenotype was determined to be due to perturbation of the endoplasmic reticulum attributed to the slow-folding nature of the pendrin protein (46). Mutations in pendrin that lead to its retention in the endoplasmic reticulum are associated with Pendred syndrome, an autosomal recessive disorder characterized by congenital deafness and goiter (46). To date, no genetic disorders have been described that map the location of the human SLC37A2 gene, 11q24.2.

Our identification of Slc37a2 transcript was based on its differential expression between WAT depots and we demonstrated that an enrichment of adipose tissue macrophages in the EP depot likely accounts for the approximately twofold upregulation of Slc37a2 transcript we observe in EP vs. SC *ob/ob* WAT depots. This is in line with the reports that intra-abdominal adipose tissue expresses increased levels of the chemokine MCP-1 (11), a key signal in macrophage infiltration, and that transgene-driven expression of MCP-1 in adipose tissue results in increased macrophage infiltration (32). With the assumption that *emr1* expression tracks closely with macrophage number irrespective of WAT depot type, the upregulation of Slc37a2 transcript we describe between *ob/ob* and wild-type WAT would be only partly explained by the increased numbers of macrophages that are present in *ob/ob* vs. wild-type WAT and/or are capable of infiltrating the tissue. Our data support the notion that the Slc37a2 transcript appears to be differentially upregulated specifically in the subpopulation of macrophages that infiltrate WAT in obesity. As such, our findings would also lead to the assertion that the subpopulation of macrophage cell type(s) found in *ob/ob* WAT may be molecularly distinct from that found in wild-type WAT. Our data indicate that *emr1*-positive macrophages in *ob/ob* WAT express elevated levels of Slc37a2 transcript compared with *emr1*-positive macrophages present in wild-type WAT. This indicates that a unique subpopulation of macrophages, rather than those typically resident in wild-type WAT, appears to infiltrate WAT under conditions of obesity. This idea is in line with a report that macrophage infiltration into WAT is attributed to migration from bone marrow (56).

It has been proposed that increased local macrophage number in obese WAT likely contributes to the spectrum of inflammatory mediators present in obesity, many of these linked to the systemic detrimental effects of obesity on health (39). We postulate that Slc37a2 possesses a sugar transporter function that is particularly required for those macrophages that are present in obese WAT. Modulation of Slc37a2 expression and/or function in macrophages may serve as an intervention point to limit the contribution of macrophages present in obese adipose tissue to the chronic inflammatory state present in obesity. Future studies from this laboratory will address the function of the Slc37a2 protein in macrophage metabolism and investigate its relationship to inflammation and obesity.

GRANTS

Research was supported by National Institutes of Health National Institute of Diabetes and Digestive and Kidney Diseases Grant 5R21-DK-064992 to C. M. Smas.

REFERENCES

1. Abu-Abid S, Szold A, Klausner J. Obesity and cancer. *J Med* 33: 73–86, 2002.
2. Ahima RS, Flier JS. Adipose tissue as an endocrine organ. *Trends Endocrinol Metab* 11: 327–332, 2000.
3. Ailhaud G, Grimaldi P, Negrel R. Cellular and molecular aspects of adipose tissue development. *Annu Rev Nutr* 12: 207–233, 1992.
4. Barrett MP, Walmsley AR, Gould GW. Structure and function of facilitative sugar transporters. *Curr Opin Cell Biol* 11: 496–502, 1999.
5. Bartoloni L, Antonarakis SE. The human sugar-phosphate/phosphate exchanger family SLC37. *Pflügers Arch* 447: 780–783, 2004.
6. Bartoloni L, Wattenhofer M, Kudoh J, Berry A, Shibuya K, Kawasaki K, Wang J, Asakawa S, Talior I, Bonne-Tamir B, Rossier C, Michaud J, McCabe ER, Minoshima S, Shimizu N, Scott HS, Antonarakis SE. Cloning and characterization of a putative human glycerol 3-phosphate permease gene (SLC37A1 or G3PP) on 21q22.3: mutation analysis in two candidate phenotypes, DFNB10 and a glycerol kinase deficiency. *Genomics* 70: 190–200, 2000.
7. Bjorntorp P. Abdominal obesity and the metabolic syndrome. *Ann Med* 24: 465–468, 1992.
8. Bodes AM, Varma V, Yao-Borengasser A, Phanavanh B, Peterson CA, McGehee RE Jr, Rasouli N, Wabitsch M, Kern PA. Pioglitazone induces apoptosis of macrophages in human adipose tissue. *J Lipid Res* 47: 2080–2088, 2006.
9. Bouloumie A, Curat CA, Sengenès C, Lolmede K, Miranville A, Busse R. Role of macrophage tissue infiltration in metabolic diseases. *Curr Opin Clin Nutr Metab Care* 8: 347–354, 2005.
10. Bruun JM, Helge JW, Richelsen B, Stallknecht B. Diet and exercise reduce low-grade inflammation and macrophage infiltration in adipose tissue but not in skeletal muscle in severely obese subjects. *Am J Physiol Endocrinol Metab* 290: E961–E967, 2006.
11. Bruun JM, Lihn AS, Pedersen SB, Richelsen B. Monocyte chemoattractant protein-1 release is higher in visceral than subcutaneous human adipose tissue (AT): implication of macrophages resident in the AT. *J Clin Endocrinol Metab* 90: 2282–2289, 2005.
12. Calle EE, Kaaks R. Overweight, obesity and cancer: epidemiological evidence and proposed mechanisms. *Nat Rev Cancer* 4: 579–591, 2004.
13. Camp HS, Ren D, Leff T. Adipogenesis and fat-cell function in obesity and diabetes. *Trends Mol Med* 8: 442–447, 2002.
14. Canello R, Henegar C, Viguier N, Taleb S, Poitou C, Rouault C, Coupaye M, Pelloux V, Hugol D, Bouillot JL, Bouloumie A, Barbatelli G, Cinti S, Svensson PA, Barsh GS, Zucker JD, Basdevant A, Langin D, Clement K. Reduction of macrophage infiltration and chemoattractant gene expression changes in white adipose tissue of morbidly obese subjects after surgery-induced weight loss. *Diabetes* 54: 2277–2286, 2005.
15. Canello R, Tordjman J, Poitou C, Guilhem G, Bouillot JL, Hugol D, Coussieu C, Basdevant A, Hen AB, Bedossa P, Guerre-Millo M, Clement K. Increased infiltration of macrophages in omental adipose tissue is associated with marked hepatic lesions in morbid human obesity. *Diabetes* 55: 1554–1561, 2006.
16. Caserta F, Tchkonja T, Civelek VN, Prentki M, Brown NF, McGarry JD, Forse RA, Corkey BE, Hamilton JA, Kirkland JL. Fat depot origin affects fatty acid handling in cultured rat and human preadipocytes. *Am J Physiol Endocrinol Metab* 280: E238–E247, 2001.
17. Charriere G, Cousin B, Arnaud E, Andre M, Bacou F, Penicaud L, Casteilla L. Preadipocyte conversion to macrophage. Evidence of plasticity. *J Biol Chem* 278: 9850–9855, 2003.
18. Chou JY. The molecular basis of type 1 glycogen storage diseases. *Curr Mol Med* 1: 25–44, 2001.
19. Christiansen T, Richelsen B, Bruun JM. Monocyte chemoattractant protein-1 is produced in isolated adipocytes, associated with adiposity and reduced after weight loss in morbid obese subjects. *Int J Obes* 29: 146–150, 2005.
20. Cinti S, Mitchell G, Barbatelli G, Murano I, Ceresi E, Faloia E, Wang S, Fortier M, Greenberg AS, Obin MS. Adipocyte death defines macrophage localization and function in adipose tissue of obese mice and humans. *J Lipid Res* 46: 2347–2355, 2005.
21. Coppack SW. Proinflammatory cytokines and adipose tissue. *Proc Nutr Soc* 60: 349–356, 2001.
22. Cousin B, Munoz O, Andre M, Fontanilles AM, Dani C, Cousin JL, Laharrague P, Casteilla L, Penicaud L. A role for preadipocytes as macrophage-like cells. *FASEB J* 13: 305–312, 1999.
23. Curat CA, Wegner V, Sengenès C, Miranville A, Tonus C, Busse R, Bouloumie A. Macrophages in human visceral adipose tissue: increased accumulation in obesity and a source of resistin and visfatin. *Diabetologia* 49: 744–747, 2006.
24. Despres JP. Is visceral obesity the cause of the metabolic syndrome? *Ann Med* 38: 52–63, 2006.
25. Di Gregorio GB, Yao-Borengasser A, Rasouli N, Varma V, Lu T, Miles LM, Ranganathan G, Peterson CA, McGehee RE, Kern PA. Expression of CD68 and macrophage chemoattractant protein-1 genes in human adipose and muscle tissues: association with cytokine expression, insulin resistance, and reduction by pioglitazone. *Diabetes* 54: 2305–2313, 2005.
26. Gerin I, Veiga-da-Cunha M, Achouri Y, Collet JF, Van Schaftingen E. Sequence of a putative glucose 6-phosphate translocase, mutated in glycogen storage disease type Ib. *FEBS Lett* 419: 235–238, 1997.

27. **Giorgino F, Laviola L, Eriksson JW.** Regional differences of insulin action in adipose tissue: insights from in vivo and in vitro studies. *Acta Physiol Scand* 183: 13–30, 2005.
28. **Greenberg AS, Obin MS.** Obesity and the role of adipose tissue in inflammation and metabolism. *Am J Clin Nutr* 83: 461S–465S, 2006.
29. **Gregoire FM, Smas CM, Sul HS.** Understanding adipocyte differentiation. *Physiol Rev* 78: 783–809, 1998.
30. **Hotamisligil GS.** Inflammatory pathways and insulin action. *Int J Obes Relat Metab Disord* 27, Suppl 3: S53–S55, 2003.
31. **Huang Y, Lemieux MJ, Song J, Auer M, Wang DN.** Structure and mechanism of the glycerol-3-phosphate transporter from *Escherichia coli*. *Science* 301: 616–620, 2003.
32. **Kanda H, Tateya S, Tamori Y, Kotani K, Hiasa K, Kitazawa R, Kitazawa S, Miyachi H, Maeda S, Egashira K, Kasuga M.** MCP-1 contributes to macrophage infiltration into adipose tissue, insulin resistance, and hepatic steatosis in obesity. *J Clin Invest* 116: 1494–1505, 2006.
33. **Khazen W, M'Bika JP, Tomkiewicz C, Benelli C, Chany C, Achour A, Forest C.** Expression of macrophage-selective markers in human and rodent adipocytes. *FEBS Lett* 579: 5631–5634, 2005.
34. **Kirkland JL, Hollenberg CH, Gillon WS.** Effects of fat depot site on differentiation-dependent gene expression in rat preadipocytes. *Int J Obes Relat Metab Disord* 20, Suppl 3: S102–S107, 1996.
35. **Klaus S, Keijer J.** Gene expression profiling of adipose tissue: individual, depot-dependent, and sex-dependent variabilities. *Nutrition* 20: 115–120, 2004.
36. **Laborda J.** 36B4 cDNA used as an estradiol-independent mRNA control is the cDNA for human acidic ribosomal phosphoprotein PO. *Nucleic Acids Res* 19: 3998, 1991.
37. **Larson TJ, Schumacher G, Boos W.** Identification of the glpT-encoded sn-glycerol-3-phosphate permease of *Escherichia coli*, an oligomeric integral membrane protein. *J Bacteriol* 152: 1008–1021, 1982.
38. **Lee YH, Nair S, Rousseau E, Allison DB, Page GP, Tataranni PA, Bogardus C, Permana PA.** Microarray profiling of isolated abdominal subcutaneous adipocytes from obese vs. non-obese Pima Indians: increased expression of inflammation-related genes. *Diabetologia* 48: 1776–1783, 2005.
39. **Lehrke M, Lazar MA.** Inflamed about obesity. *Nat Med* 10: 126–127, 2004.
40. **Leuzzi R, Fulceri R, Marcolongo P, Banhegyi G, Zammarchi E, Stafford K, Burchell A, Benedetti A.** Glucose 6-phosphate transport in fibroblast microsomes from glycogen storage disease type 1b patients: evidence for multiple glucose 6-phosphate transport systems. *Biochem J* 357: 557–562, 2001.
41. **Marger MD, Saier MH Jr.** A major superfamily of transmembrane facilitators that catalyze uniport, symport and antiport. *Trends Biochem Sci* 18: 13–20, 1993.
42. **Montague CT.** Adipose depot-specific effects of PPAR gamma agonists: a consequence of differential expression of PPAR gamma in adipose tissue depots? *Diabetes Obes Metab* 4: 356–361, 2002.
43. **Narisawa K, Otomo H, Igarashi Y, Arai N, Otake M, Tada K, Kuzuya T.** Glycogen storage disease type 1b due to a defect of glucose-6-phosphate translocase. *J Inherit Metab Dis* 5: 227–228, 1982.
44. **Neels JG, Olefsky JM.** Inflamed fat: what starts the fire? *J Clin Invest* 116: 33–35, 2006.
45. **Permana PA, Menge C, Reaven PD.** Macrophage-secreted factors induce adipocyte inflammation and insulin resistance. *Biochem Biophys Res Commun* 341: 507–514, 2006.
46. **Shepshelovich J, Goldstein-Magal L, Globerson A, Yen PM, Rotman-Pikielny P, Hirschberg K.** Protein synthesis inhibitors and the chemical chaperone TMAO reverse endoplasmic reticulum perturbation induced by overexpression of the iodide transporter pendrin. *J Cell Sci* 118: 1577–1586, 2005.
47. **Skurk T, Herder C, Kraft I, Muller-Scholze S, Hauner H, Kolb H.** Production and release of macrophage migration inhibitory factor from human adipocytes. *Endocrinology* 146: 1006–1011, 2005.
48. **Smas CM, Chen L, Sul HS.** Cleavage of membrane-associated pref-1 generates a soluble inhibitor of adipocyte differentiation. *Mol Cell Biol* 17: 977–988, 1997.
49. **Takahashi K, Mizuarai S, Araki H, Mashiko S, Ishihara A, Kanatani A, Itadani H, Kotani H.** Adiposity elevates plasma MCP-1 levels leading to the increased CD11b-positive monocytes in mice. *J Biol Chem* 278: 46654–46660, 2003.
50. **Tchkonian T, Giorgadze N, Pirtskhalava T, Tchoukalova Y, Karagiannides I, Forse RA, DePonte M, Stevenson M, Guo W, Han J, Waloga G, Lash TL, Jensen MD, Kirkland JL.** Fat depot origin affects adipogenesis in primary cultured and cloned human preadipocytes. *Am J Physiol Regul Integr Comp Physiol* 282: R1286–R1296, 2002.
51. **Todoric J, Loffler M, Huber J, Bilban M, Reimers M, Kadl A, Zeyda M, Waldhausl W, Stulnig TM.** Adipose tissue inflammation induced by high-fat diet in obese diabetic mice is prevented by n-3 polyunsaturated fatty acids. *Diabetologia* In press.
52. **Vidal H.** Gene expression in visceral and subcutaneous adipose tissues. *Ann Med* 33: 547–555, 2001.
53. **Villena JA, Cousin B, Penicaud L, Casteilla L.** Adipose tissues display differential phagocytic and microbicidal activities depending on their localization. *Int J Obes Relat Metab Disord* 25: 1275–1280, 2001.
54. **Wajchenberg BL, Giannella-Neto D, da Silva ME, Santos RF.** Depot-specific hormonal characteristics of subcutaneous and visceral adipose tissue and their relation to the metabolic syndrome. *Horm Metab Res* 34: 616–621, 2002.
55. **Wang H, Kirkland JL, Hollenberg CH.** Varying capacities for replication of rat adipocyte precursor clones and adipose tissue growth. *J Clin Invest* 83: 1741–1746, 1989.
56. **Weisberg SP, McCann D, Desai M, Rosenbaum M, Leibel RL, Ferrante AW Jr.** Obesity is associated with macrophage accumulation in adipose tissue. *J Clin Invest* 112: 1796–1808, 2003.
57. **Wellen KE, Hotamisligil GS.** Inflammation, stress, diabetes. *J Clin Invest* 115: 1111–1119, 2005.
58. **Wellen KE, Hotamisligil GS.** Obesity-induced inflammatory changes in adipose tissue. *J Clin Invest* 112: 1785–1788, 2003.
59. **Xu H, Barnes GT, Yang Q, Tan G, Yang D, Chou CJ, Sole J, Nichols A, Ross JS, Tartaglia LA, Chen H.** Chronic inflammation in fat plays a crucial role in the development of obesity-related insulin resistance. *J Clin Invest* 112: 1821–1830, 2003.